Monthly Notices
of the
ROYAL ASTRONOMICAL SOCIETY

MNRAS **446,** 4019–4028 (2015) doi:10.1093/mnras/stu2350

The High Time Resolution Universe survey – XI. Discovery of five recycled pulsars and the optical detectability of survey white dwarf companions

S. D. Bates,[1,2★] D. Thornton,[1,3] M. Bailes,[4,5] E. Barr,[5,6] C. G. Bassa,[7] N. D. R. Bhat,[4,5,8] M. Burgay,[9] S. Burke-Spolaor,[10,11] D. J. Champion,[6] C. M. L. Flynn,[4,5] A. Jameson,[4] S. Johnston,[3] M. J. Keith,[1] M. Kramer,[1,6] L. Levin,[12] A. Lyne,[1] S. Milia,[9,13] C. Ng,[6] E. Petroff,[3,4,5] A. Possenti,[9] B. W. Stappers,[1] W. van Straten[4,5] and C. Tiburzi[3,13]

[1]*Jodrell Bank Centre for Astrophysics, School of Physics and Astronomy, The University of Manchester, Manchester M13 9PL, UK*
[2]*National Radio Astronomy Observatory, PO Box 2, Green Bank, WV 24944, USA*
[3]*CSIRO Astronomy & Space Science, Australia Telescope National Facility, PO Box 76, Epping, NSW 1710, Australia*
[4]*Centre for Astrophysics and Supercomputing, Swinburne University of Technology, PO Box 218, Hawthorn, VIC 3122, Australia*
[5]*ARC Centre of Excellence for All-Sky Astronomy (CAASTRO), Mail H30, Swinburne University of Technology, PO Box 218, Hawthorn, VIC 3122, Australia*
[6]*MPI fuer Radioastronomie, Auf dem Huegel 69, D-53121 Bonn, Germany*
[7]*ASTRON, the Netherlands Institute for Radio Astronomy, Postbus 2, NL-7990 AA Dwingeloo, the Netherlands*
[8]*Iternational Centre for Radio Astronomy Research, Curtin University, Bentley, WA 6102, Australia*
[9]*INAF – Osservatorio Astronomico di Cagliari, via della Scienza 5, I-09047 Selargius, Italy*
[10]*NASA Jet Propulsion Laboratory, M/S 138-307, Pasadena, CA 91106, USA*
[11]*California Institute of Technology, 1200 E California Blvd, Pasadena, CA, 91125, USA*
[12]*Department of Physics and Astronomy, West Virginia University, Morgantown, WV 26506, USA*
[13]*Dipartimento di Fisica, Università degli Studi di Cagliari, Cittadella Universitaria, I-09042 Monserrato (CA), Italy*

Accepted 2014 November 3. Received 2014 November 3; in original form 2014 September 22

ABSTRACT

We present the discovery of a further five recycled pulsar systems in the mid-Galactic latitude portion of the High Time Resolution Universe survey. The pulsars have rotational periods ranging from 2 to 66 ms, and four are in binary systems with orbital periods between 10.8 h and 9 d. Three of these binary systems are particularly interesting; PSR J1227−6208 has a pulse period of 34.5 ms and the highest mass function of all pulsars with near-circular orbits. The circular orbit suggests that the companion is not another neutron star, so future timing experiments may reveal one of the heaviest white dwarfs ever found ($>1.3\ M_\odot$). Timing observations of PSR J1431−4715 indicate that it is eclipsed by its companion which has a mass indicating it belongs to the redback class of eclipsing millisecond pulsars. PSR J1653−2054 has a companion with a minimum mass of only $0.08\ M_\odot$, placing it among the class of pulsars with low-mass companions. Unlike the majority of such systems, however, no evidence of eclipses is seen at 1.4 GHz.

Key words: methods: data analysis – stars: neutron – pulsars: general.

1 INTRODUCTION

Although pulsars are commonly born with short spin periods (e.g. Migliazzo et al. 2002, and references therein), the spin-down rate is such that pulsars are often observed to have spin periods of the order of 1 s. However, the millisecond pulsars (MSPs) spin with periods $\lesssim$30 ms. The MSPs are located in a region of the P–$\dot{P}$ diagram distinct from *ordinary* pulsars. In order to be rotating so rapidly, MSPs are thought to have undergone a spin-up phase in their evolutionary history. Spin-up involves accretion of matter from an orbiting companion on to the neutron star (NS; Alpar et al. 1982), which begins when the companion star ages and expands, in some cases, to overflow its Roche lobe. During the accretion phase, systems are thought to be observed as X-ray binaries, both as high-mass (HMXB) and low-mass X-ray binaries (LMXB) depending upon the companion mass.

The evolutionary link between X-ray binaries and MSPs was strengthened with the discovery of SAX J1808.4−3658, an X-ray binary exhibiting periodic intensity fluctuations with a

★ E-mail: sam.d.bates@gmail.com

period of 2.4 ms (Wijnands & van der Klis 1998). More recently, PSR J1023+0038 was argued to have switched from an LMXB to a radio pulsar phase (Archibald et al. 2009), and now has undergone a transition back to an LMXB (Stappers et al. 2014). The radio pulsar J1824−2425I was the first to be observed to switch to an LMXB phase for a period of around a month, before radio pulsations were once again detected (Papitto et al. 2013). All three systems further strengthen the spin-up model of MSP formation.

Some HMXBs may have a donor sufficiently massive to undergo a core-collapse supernova (ccSN), providing a strong kinematic kick to the system. This kick and mass-loss from the companion will either disrupt the binary totally or impart a significant eccentricity to the orbit (Chaurasia & Bailes 2005). What remains is therefore either an eccentric double neutron star (DNS) system, for example PSR B1913+16 (Hulse & Taylor 1975) and PSR J0737−3039 (Burgay et al. 2003; Lyne et al. 2004), or two separate NSs. In both cases, one NS has undergone a spin-up phase (the recycled pulsar) while the other is a young NS (either of which may be observable as a pulsar).

The LMXBs are systems where the companion has a lower mass than the pulsar. The companions reach the end of their lives as a red giant with expulsion of the outer layers of the star, leaving a degenerate core – a white dwarf (WD). The long-lived period ($\sim 10^8$ yr; Tauris & van den Heuvel 2003) of stable mass transfer acts to circularize the orbit after the ccSN of the NS progenitor (Bhattacharya & van den Heuvel 1991), explaining why Galactic field MSP–WD binaries usually have a low orbital eccentricity (Phinney 1992).

The fact that most MSPs are found in binaries is in agreement with the spin-up evolutionary scenario; however, ∼20 per cent of observed MSPs in the Galactic field are isolated. Besides the formation of isolated MSPs from disruption of the orbit during a second ccSN as the HMXB phase ends, MSPs may destroy their companions through ablation due to the wind from the pulsar (Ruderman, Shaham & Tavani 1989). Systems undergoing this process are known as *black widow* systems (Fruchter, Stinebring & Taylor 1988), consisting of an MSP with an ultralow-mass companion ($M_c \approx 0.02\,M_\odot$). Radio emission from the pulsar is sometimes observed to be eclipsed by ionized material surrounding the companion and, if the orbital inclination is favourable, the companion itself (for example PSR B1957+20; Fruchter et al. 1988). The timescale for total ablation of the companion is, however, too long to explain the observed number of isolated MSPs (Eichler & Levinson 1988). So-called *redback* binary systems (Roberts 2011), such as PSR J1740−5340A in globular cluster NGC 6397, also exhibit orbital eclipses of the pulsar emission (D'Amico et al. 2001). Redback systems have a more massive companion, ($M_c \sim 10^{-1} M_\odot$) often seen to be non-degenerate in optical studies (Roberts 2011). These systems have Roche lobe filling factors of 0.1–0.4, and as such are possibly an interesting intermediate stage between X-ray binaries and Galactic field MSP binary systems (Breton et al. 2013).

Using the 64 m Parkes radio telescope the High Time Resolution Universe (HTRU) survey (Keith et al. 2010) is providing a comprehensive search of the entire southern sky with high time and frequency resolution for pulsars. It uses the 20 cm multibeam receiver which was also used by the Parkes Multibeam Pulsar Survey (PMPS; Manchester et al. 2001) combined with a digital backend system with superior spectral and temporal resolution to the analogue filterbank system used in the PMPS.

This paper outlines the discovery and subsequent observation of five recycled pulsar systems. Section 2 outlines the observations taken to discover and observe these pulsars. In Section 3, we present the results of our timing programme to date, including details of the pulse profiles and, where possible, multifrequency observations. Finally, in Section 4, we present calculations of predicted WD optical brightnesses for all published MSP–WD systems discovered in the HTRU survey.

Table 1. Observing system details for the timing observations made as part of this work; observing bandwidth, BW, number of frequency channels, $n_{\rm chan}$, and mean observation length, $\langle \tau_{\rm obs} \rangle$. Note the specifications for the Lovell telescope take into account the removal, as standard, of a section of the observing bandwidth due to contamination by radio-frequency interference (RFI).

Telescope	Centre freq. (GHz)	BW (GHz)	$n_{\rm chan}$	$\langle \tau_{\rm obs} \rangle$ (s)
Parkes 64 m	0.732	0.064	512	900
	1.369	0.256	1024	600
	3.094	1.024	1024	900
Lovell 76 m	1.524	0.384	768	1800

2 DISCOVERY AND TIMING

The five pulsars presented here were discovered in the HTRU survey for pulsars and transients (for a full discussion, see Keith et al. 2010). Survey observations were made with the 64 m Parkes radio telescope using the 13 beam 21 cm multibeam receiver. The survey has an observing band centred at 1352 MHz and has a useful bandwidth of 340 MHz. The HTRU survey is split into three areas: the low-, mid- and high-Galactic latitude regions. The discoveries presented here are from the mid-latitude survey, which tiles $-120^\circ < l < 30^\circ$ and $|b| \leq 15^\circ$ with observations of 540 s.

The data were processed using the Fourier transform based pulsar search pipeline described in Keith et al. (2010). The discoveries presented here were initially identified using an artificial neural network which aims to highlight the best candidates from the survey for human inspection (Eatough et al. 2010; Bates et al. 2012). After inspection, confirmation observations were taken at the sky positions of the survey beams deemed to contain the best candidates. These confirmations were performed with the Parkes or Lovell telescopes. Four of the five pulsars presented here, PSRs J1227−6208, J1405−4656, J1431−4715, and J1653−2054, are in orbit with a binary companion, while one, PSR J1729−2117, is isolated. PSR J1227−6208 was also independently discovered in the PMPS by two separate groups (Mickaliger et al. 2012; Knispel et al. 2013). All observations, timing, and analysis of PSR J1227−6208 presented here are independent work.

After confirmation, the new pulsars were timed regularly with digital filter bank backend systems; PSRs J1653−2054 and J1729−2117 with the 76 m Lovell telescope at Jodrell Bank Observatory and PSRs J1431−4715, J1405−4656, and J1227−6208 with the 64m radio telescope at Parkes (see Table 1). The pulsars timed with the Lovell telescope were observed approximately once per fortnight, whereas those observed using the Parkes radio telescope were observed more sporadically, while maintaining phase coherence, with one case of an approximately 80 d gap between observations.

Each observation resulted in a pulse time-of-arrival (TOA) measurement. Parameters were fitted to the TOAs using the TEMPO2 software package (Hobbs, Edwards & Manchester 2006) and the

Table 2. Observed and derived parameters for the five MSPs. The DM distance has been estimated using the NE2001 model of Cordes & Lazio (2002), while a pulsar mass of 1.4 $M_\odot$ has been assumed in calculating companion masses. Estimates of the contribution to the period derivative from the Shklovskii effect have been included, where significant proper motions have been measured. ELL1 refers to the timing model outlined in the appendix of Lange et al. (2001) and ELL1H is a modification to this model to allow the Shapiro delay to be parametrized in terms of h_3 and h_4 (see the text and equation 3). Note all parameter errors have been multiplied by $\sqrt{\chi^2}$.

Parameter	J1227−6208	J1405−4656	J1431−4715	J1653−2054	J1729−2117
Right ascension (J2000)	12:27:00.4413(4)	14:05:21.4255(8)	14:31:44.6177(2)	16:53:31.03(2)	17:29:10.808(6)
Declination (J2000)	−62:08:43.789(3)	−46:56:02.31(1)	−47:15:27.574(4)	−20:54:55.1(1)	−21:17:28(1)
Galactic longitude (°)	300.08	315.83	320.05	359.97	4.50
Galactic latitude (°)	0.59	14.08	12.25	−14.26	7.22
Discovery signal-to-noise ratio	11.2	125.0	12.0	11.5	13.7
Offset from survey Beam centre (arcmin)	6	3	1.8	2.4	4.8
TOA range (MJD)	55901–56641	55668–56557	55756–56627	55658–56676	55505–56686
P (ms)	34.527 834 647 80(2)	7.602 203 432 51(1)	2.011 953 442 5332(9)	4.129 145 284 562(2)	66.292 899 2668(4)
$\dot{P}_{\rm meas}$ ($\times 10^{-20}$)	18.74(7)	2.79(4)	1.411(3)	1.117(6)	17.2(7)
$\dot{P}_{\rm Shk}$ ($\times 10^{-20}$)	–	2(1)	0.09(7)	–	–
$\dot{P}_{\rm meas} - \dot{P}_{\rm shk}$ ($\times 10^{-20}$)	18.74(7)	1(1)	1.32(9)	1.117(6)	17.2(7)
DM ($\rm cm^{-3}$ pc)	363.0(2)	13.884(3)	59.35(1)	56.56(2)	34.49(4)
DM distance (kpc)	8.32	0.58	1.53	1.63	1.09
$S_{1.4\,\rm GHz}$ (mJy)	0.22	0.92	0.73	0.16	0.20
$L_{1.4\,\rm GHz}$ (mJy $\rm kpc^2$)	15.2	0.3	1.7	0.4	0.02
$\tau_{\rm c}$ (10^9 yr)	2.9	36	2.3	5.9	6.1
$B_{\rm surf}$ (G)	2.6×10^9	1.6×10^8	1.7×10^8	2.2×10^8	3.4×10^9
$B_{\rm lc}$ (G)	5.7×10^2	3.3×10^3	1.9×10^5	2.8×10^4	1.1×10^2
$\dot{E}$ (erg $\rm s^{-1}$)	1.8×10^{32}	3.0×10^{32}	6.8×10^{34}	6.3×10^{33}	2.3×10^{31}
$\dot{E}/d^2$ (erg $\rm kpc^{-2}$ $\rm s^{-1}$)	2.6×10^{30}	8.9×10^{32}	2.9×10^{34}	2.4×10^{33}	1.9×10^{31}
Proper motion:					
$\mu_{\rm RA}$ (mas $\rm yr^{-1}$)	–	−44(6)	−7(3)	–	–
$\mu_{\rm Dec}$ (mas $\rm yr^{-1}$)	–	20(10)	−8(4)	–	–
$\mu_{\rm Total}$ (mas $\rm yr^{-1}$)	–	48(8)	11(4)	–	–
Binary model	ELL1H	ELL1	ELL1	ELL1	–
Orbital period (d)	6.721 013 337(4)	8.956 419 88(7)	0.449 739 1377(7)	1.226 815 259(9)	–
$a\sin i$ (ls)	23.200 663(3)	6.567 659(9)	0.550 061(2)	0.688 855(6)	–
TASC (MJD)	55991.1937918(2)	55132.23096(2)	55756.1047771(4)	55584.728649(3)	–
$T0$ (MJD)	55991.7000(2)	55694.0(4)	55756.23(2)	55584.9(5)	–
ϵ_1	0.000 5238(3)	0.000 005(2)	0.000 023(8)	0.000 00(2)	–
ϵ_2	0.001 0229(3)	0.000 004(2)	−0.000 003(7)	0.000 00(2)	–
e	0.001 1494(3)	0.000 007(2)	0.000 023(8)	0.000 01(3)	–
ω (deg)	27.11(1)	51(16)	97(18)	0(30)	–
Shapiro delay parameters					
h_3 ($\times 10^{-6}$)	7.3 ± 2.7	–	–	–	–
h_4 ($\times 10^{-6}$)	4.4 ± 3.2	–	–	–	–
Min. $m_{\rm c}$ ($M_\odot$)	1.27	0.21	0.12	0.08	–
Med. $m_{\rm c}$ ($M_\odot$)	1.58	0.25	0.14	0.09	–
rms of fit (μs)	22	26	10	35	162
Reduced χ^2	1.30	1.05	1.8*	1.7	2.7
PEPOCH	55991.2	55692.7	55756.1	55694.6	55505

*When TOAs around superior conjunction are removed.

best-fitting parameters for the five recycled pulsars are given in Table 2.

3 RESULTS

The pulse periods for the new discoveries range from 2.01 ms for PSR J1431−4715, placing it among the 20 fastest spinning pulsars, to 66.29 ms for PSR J1729−2117, one of the longer periods for a partially recycled pulsar (Manchester et al. 2005).[1] One, PSR J1729−2117, has not exhibited any detectable periodic variation of the pulse period over the three years of timing, indicating that it is one of just two isolated recycled pulsars discovered in the HTRU

[1] www.atnf.csiro.au/people/pulsar/psrcat

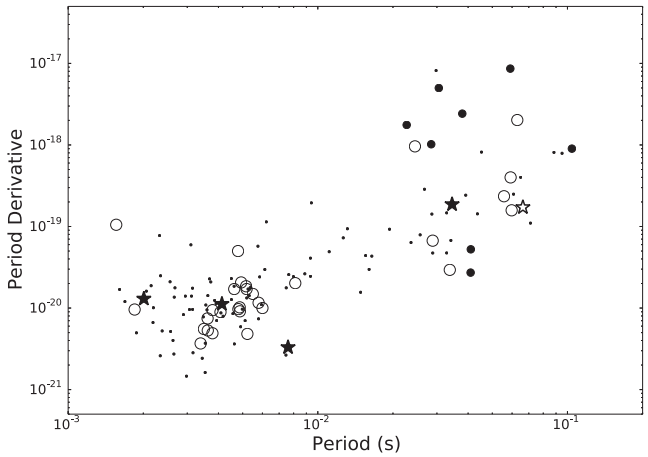

Figure 1. A plot of pulse period derivative, $\dot{P}$, against pulse period, P, using the intrinsic values of $\dot{P}$ given in Table 1. DNS systems (see Table 3) are plotted as large filled circles, other binaries are small filled circles, and isolated systems are unfilled circles. The discoveries presented in this work are shown as stars, with the isolated system PSR J1729−2117 an unfilled star. Only non-globular cluster pulsars with $P < 100$ ms and $\dot{P} < 10^{-16}$ and DNS systems are shown.

survey to date. The five pulsars represent some of the different types of known recycled pulsar and binary systems.

3.1 Period derivatives

The measured spin-down rate, $\dot{P}_{\rm meas}$, of a pulsar with period P can differ from the intrinsic spin-down via the Shklovskii effect (Shklovskii 1970). A proper motion of μ, for a pulsar with period P at distance d, leads to an extra contribution to the period derivative as

$$\dot{P}_{\rm Shk} \simeq 2.43 \times 10^{-21} \left(\frac{P}{\rm s}\right) \times \left(\frac{\mu^2}{\rm mas\,yr^{-1}}\right) \times \left(\frac{d}{\rm kpc}\right), \qquad (1)$$

where c is in units of m s^{-1}, which can be a considerable contribution for some MSPs since their rotational periods are so short, the measured $\dot{P}$ so small, and transverse velocities are typically ∼85 km s^{-1} (Toscano et al. 1999). This being the case, the Shklovskii effect is likely to give only small contributions (of the order $\lesssim$10 per cent) to the measured $\dot{P}$ for PSRs J1227−6208 and J1653−2054 (for which no significant proper motion has been measured), but for PSR J1729−2117, the Shklovskii effect could easily contribute a significant fraction, $\gtrsim$ 30 per cent, of the measured $\dot{P}$.

In the cases of PSRs J1405−4656 and J1431−4715, which have measured, significant proper motions of 48 and 11 mas yr^{-1}, respectively. The Shklovskii effect then contributes ∼90 and ∼5 per cent of the measured $\dot{P}$ for these pulsars. In Table 2, we include corrections for the Shklovskii effect, where it may be calculated. However, the errors on the value of $\dot{P}_{\rm Shk}$ (and, hence, the intrinsic period derivative) are rather large, especially in the case of PSR J1405−4656, due mainly to contributions from the error on the proper motion and the distance derived from the electron distribution model, which we have assumed to be 30 per cent.

3.2 PSR J1227−6208

PSR J1227−6208 is located in the region of the P–$\dot{P}$ diagram where mildly recycled pulsars are found (see Fig. 1). This is consistent with it having been spun-up during unstable, short-lived mass transfer in an HMXB phase. Pulse profiles from observations at 1.4 and 3.1 GHz are shown in Fig. 2.

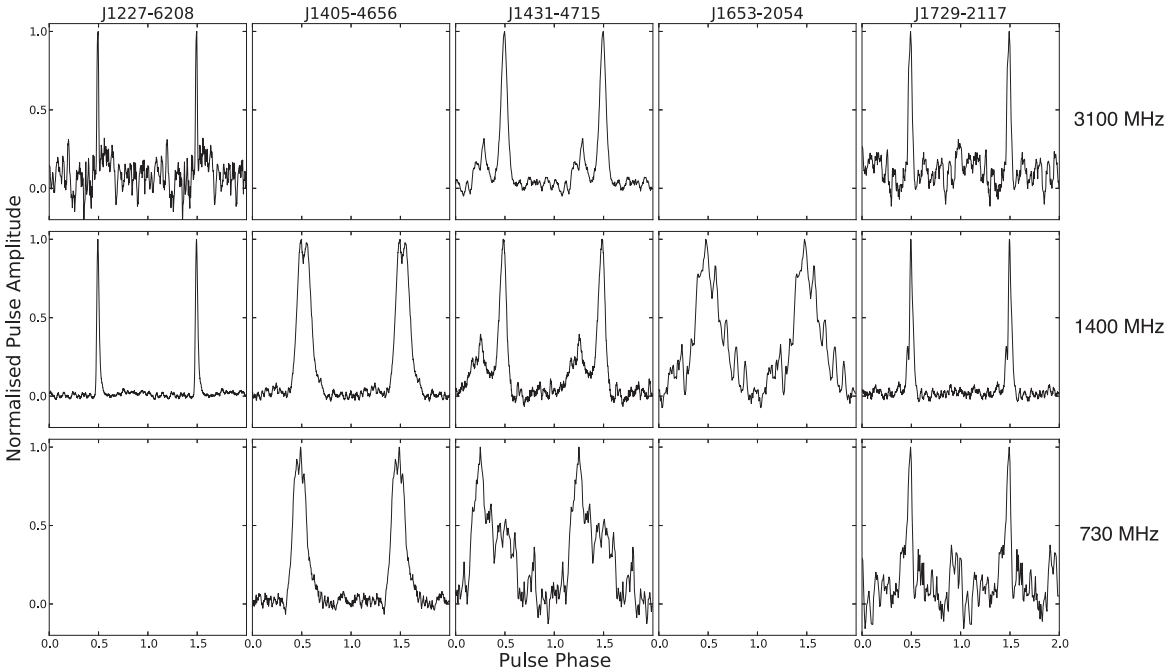

Figure 2. Typical pulse profiles are shown for the five MSPs presented here, from single observations. Profiles have been shifted so that the peaks of the 1400 MHz profile sits at a pulse phase of 0.5. Top, middle, and bottom rows correspond to observing frequencies of 3100, 1400, and 730 MHz, respectively. Blank plots correspond to non-detections. The observing times are given in Table 1. All observations are taken with the 64 m Parkes radio telescope, except for the 1.4 GHz observations and timing of PSRs J1653− 2054 and J1729− 2117, which use the 76 m Lovell telescope at Jodrell Bank.

Table 3. Basic orbital and spin parameters for known DNS systems. Also included are the same parameters for PSR J1227−6208.

Pulsar	P (ms)	$P_{\rm orb}$ (d)	$a_{\rm p}\sin i$ (ls)	e	$M_{\rm c}$ ($M_\odot$)
J0737−3039	22.69	0.102	1.415	0.088	1.250
J1518+4904	40.93	8.634	20.044	0.249	>0.83
B1534+12	37.90	0.420	3.729	0.273	1.34
J1756−2251	28.46	0.319	2.756	0.180	1.18
J1811−1736	104.18	18.779	34.783	0.828	>0.87
J1829+2456	41.00	1.176	7.236	0.139	>1.22
B1913+16	59.03	0.322	2.341	0.617	1.38
B2127+11C	30.52	0.335	2.518	0.681	1.354
J1227−6208	35.52	6.721	23.200	0.001	>1.29

It has an orbital eccentricity, $e = 0.001\,15$, orbital period $P_{\rm orb} = 6.72$ d, and a projected semimajor axis, $a_{\rm p}\sin(i) = 23.2$ls. Assuming $M_{\rm p} = 1.4\,{\rm M}_\odot$, this leads to a minimum companion mass of $M_{\rm c,\,min} = 1.29\,{\rm M}_\odot$ for an edge-on orbit. The low eccentricity and high minimum companion mass are unusual: there are only three other systems known with $e < 0.1$ and $M_{\rm c,\,min} > 1.0\,{\rm M}_\odot$.

PSR J1227−6208 is similar to other so-called intermediate-mass binary pulsars (IMBPs); for example PSR J1435−6100 (Camilo et al. 2001) and PSR J2222−0137 (Boyles et al. 2013). PSR J1227−6208's spin parameters are also similar to PSR J0609+2130 – an isolated pulsar thought to be the result of an HMXB which disrupted during the second ccSN (Lorimer et al. 2004). In an IMBP, it is thought that the companion was not sufficiently massive to undergo a ccSN, resulting instead in the formation of a heavy CO or ONeMg WD. The minimum mass for the companion to PSR J1227−6208 is common for ONeMg WDs, which have a mass range of around 1.1–1.3 $\rm M_\odot$ (Tauris, Langer & Kramer 2012). This is, however, the *minimum* mass the companion may have; it is already close to the upper limit of ONeMg WDs, and to the Chandrasekhar mass limit.

For inclinations $i < 71^\circ$, $M_{\rm c} \gtrsim 1.4\,{\rm M}_\odot$, and therefore PSR J1227−6208 might be part of a DNS system. If the companion is an NS, though not one which is visible to date as a pulsar, it would have formed from a massive progenitor (8–10 $\rm M_\odot$), and the system would have evolved through an HMXB phase, hence leaving PSR J1227−6208 partially recycled. Compared to the known DNS systems, listed in Table 3, the eccentricity is small, and the formation of DNS systems with such a small eccentricity appears to be unlikely (Chaurasia & Bailes 2005). Simulations by Dewi, Podsiadlowski & Pols (2005) and Chaurasia & Bailes (2005) do, however, suggest that such low-eccentricity DNS systems could exist because of the possibility of very small and retrograde ccSN kinematic kicks, although they would be extremely rare.

Due to the loss of binding energy ($\delta M \gtrsim 0.1\,{\rm M}_\odot$) during an SN explosion, the mass-loss induces a finite eccentricity, $e = (M + \delta M)/M - 1 \gtrsim 0.035$, into the system, which is ∼30 times that of PSR J1227−6208. The only way this can be lessened is if the exploding star receives a retrograde kick into an exceptionally small volume of phase space to reduce the angular momentum and, hence, eccentricity (Chaurasia & Bailes 2005). For NSs receiving a random kick from a large kick velocity distribution, the probability is vanishingly small (<0.1 per cent), but the double pulsar's eccentricity of 0.09 (Lyne et al. 2004) demonstrates that not all NSs receive large kicks. Even if the kick was constrained to be small and confined to the pre-SN orbital plane, PSR J1227−6208's eccentricity of 0.001 would occur less than $e_{\rm kick}/e_{\rm psr} \sim 3$ per cent of the time as most random kicks act to increase, not decrease, the orbital eccentricity induced by mass-loss. On the other hand, such low-eccentricity systems would not lose energy via gravitational wave emission as quickly as eccentric systems, and consequently will survive longer before merging.

With DM = 362.6 $\rm cm^{-3}pc$, the NE2001 electron density model predicts PSR J1227−6208 to be located at a distance of 8.3 kpc. This would make an optical detection of a WD companion (for the case of a large orbital inclination) extremely difficult. Consequently, the best chance of measuring the masses in the system comes from the potential measurement of post-Keplerian parameters.

3.2.1 *Periastron advance*

It is possible to predict relativistic changes to the orbit due to general relativity. One of the easiest post-Keplerian parameters to measure for systems with eccentric orbits is a changing longitude of periastron,

$$\dot{\omega} \simeq 39\overset{\circ}{.}73\,{\rm yr}^{-1}\left(\frac{P_{\rm orb}}{\rm h}\right)^{-5/3}\left(\frac{1}{1-e^2}\right)\left(\frac{M_{\rm c}+M_{\rm p}}{{\rm M}_\odot}\right)^{2/3}, \qquad (2)$$

where $P_{\rm orb}$ is the orbital period, e is the orbital eccentricity, and $M_{\rm c}$ and $M_{\rm p}$ are the companion and pulsar masses respectively. A measured $\dot{\omega}$ constitutes a measurement of the combined masses, $M_{\rm c} + M_{\rm p}$ and consequently constrains the companion mass. While the orbital eccentricity of PSR J1227−6208 is small, it is significantly higher than is typical for systems which have likely evolved through an LMXB phase (Phinney 1992). Equation (2) predicts $\dot{\omega} = 0\overset{\circ}{.}017\,{\rm yr}^{-1}$ for the PSR J1227−6208 system if we assume pulsar and companion masses of 1.4 $\rm M_\odot$. For a low inclination, and $M_{\rm c} = 10\,{\rm M}_\odot$, we would then expect $\dot{\omega} = 0\overset{\circ}{.}042\,{\rm yr}^{-1}$.

Current observations have not made a significant measurement of $\dot{\omega}$; however, we can make some quantitative statements about the value of $\dot{\omega}$. Using the FAKE plugin for TEMPO2, TOAs were generated for PSR J1227−6208 using the parameters listed in Table 2, varying $\dot{\omega}$ from 0.01 to $0\overset{\circ}{.}05\,{\rm yr}^{-1}$. Fitting those TOAs using TEMPO2 over the current data span, $\dot{\omega}$ was only measured at the 2σ level for $\dot{\omega} \gtrsim 0\overset{\circ}{.}04\,{\rm yr}^{-1}$. Since we are unable to make a significant measurement, it is likely that $\dot{\omega} \leq 0\overset{\circ}{.}04\,{\rm yr}^{-1}$. Extending these simulated TOAs into the future, in all cases another two years of data constrain $\dot{\omega}$ at the $\sim 3\sigma$ level, which would allow a direct measurement of $M_{\rm p}$ and $M_{\rm c}$ at the 2σ level.

3.2.2 *Shapiro delay*

The radio pulses from a pulsar in a binary system are delayed as they cross the gravitational potential of the companion in a phenomenon called Shapiro delay (Shapiro 1964). The magnitude of the delay, $\Delta_{\rm S}$, is quantified by two post-Keplerian parameters, the range, r, and the shape, s. For low-eccentricity systems

$$\Delta_{\rm S}(\Phi) = -2r\ln(1 - s\sin\Phi), \qquad (3)$$

where Φ is the orbital phase ($\Phi = 0$ is the ascending node), $r = {\rm T}_\odot M_{\rm c}$, $s = \sin i$, and ${\rm T}_\odot = {\rm GM}_\odot/c^3$. The Shapiro delay is the same for every orbit of the system and so when the TOA residuals are folded modulo-$P_{\rm orb}$ a characteristic shape in the timing residuals may be measured.

Since the companion mass for PSR J1227−6208 is relatively high, implying a large value of r, an observing programme was undertaken using the 64 m Parkes radio telescope to obtain TOAs

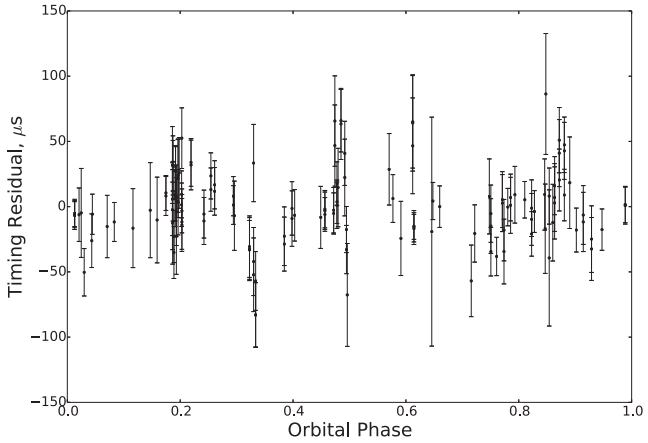

Figure 3. Timing residuals from the best-fitting global model for PSR J1227− 6208 as a function of orbital phase, without any Shapiro delay contribution taken into account. Although the timing residuals appear to show some structure, fitting for the Shapiro delay provides only marginal measurements of orbital parameters.

across the expected epoch of superior conjunction, and attempt to observe Shapiro delay in this system. A global timing solution was made (given in Table 2) using the parametrization for the Shapiro delay given by Freire & Wex (2010), where the fitted parameters h_3 and h_4 are related to the Shapiro r and s parameters as

$$r = \frac{h_3^4}{h_4^3}, \qquad s = \frac{2h_3h_4}{h_3^2 + h_4^2}. \tag{4}$$

A best-fitting value of h_3 which is consistent with zero implies a non-detection of the Shapiro delay, and a measurement of h_4 allows the orbital inclination to be constrained.

Timing residuals for PSR J1227−6208, shown in Fig. 3 were observed to show some evidence of Shapiro delay due to the apparent non-Gaussianity of the residuals. Fitting for h_3 and h_4, we obtained best-fitting values of $h_3 = (7.3 \pm 2.7) \times 10^{-6}$ and $h_4 = (4.4 \pm 3.2) \times 10^{-6}$; however, both of these measurements are to a low significance, and corresponding errors in M_c and $\sin i$ are large. Nevertheless, the resulting values of range and shape are $r = (3.3 \pm 8.8) \times 10^{-5}\,\mathrm{M}_\odot$s and $s = \sin i = 0.88^{+0.12}_{-0.33}$, respectively.

To estimate when the Shapiro delay might become well-constrained, as in Section 3.2.1, TOAs were generated for PSR J1227−6208 using the TEMPO2 plugin FAKE. Keeping the rms fixed at 22 μs, a further nine years of timing data were needed in order to constrain both h_3 and h_4 at the 3σ level. Alternatively, using the current data span, h_3 and h_4 were constrained at the 3σ level when the rms was reduced to 10 μs. Therefore, a combination of improved timing and a longer data span may enable precise measurement of h_3 and h_4 in under nine years.

3.3 PSR J1431−4715

PSR J1431−4715 has the 14th shortest spin period of all known pulsars, $P = 2.01$ ms, and a small period derivative, $\dot{P} = 1.4 \times 10^{-20}$. These values place PSR J1431−4715 firmly amongst the fully recycled MSPs in the bottom left of the P–$\dot{P}$ diagram (see Fig. 1).

Observations of PSR J1431−4715 at multiple frequencies (see Fig. 2) reveal significant pulse profile evolution with observing frequency, as well as evidence of pulse delays and eclipses when the pulsar is at superior conjunction. At 1.4 GHz, the pulse profile is double peaked, with a smaller and wider leading component,

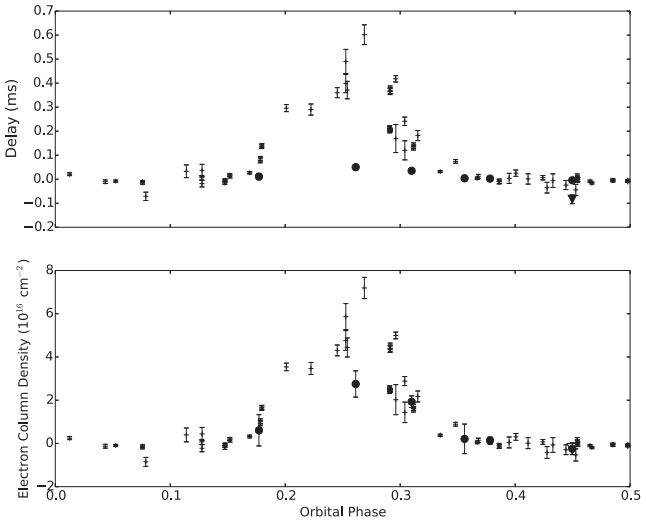

Figure 4. The top panel shows the timing residuals for PSR J1431−4715 which are folded modulo $P_{\rm orb}$, between orbital phases of 0 and 0.5. The excess residuals which are not described by the timing model are centred around superior conjunction, an orbital phase of 0.25. The lower panel shows the same delays converted to an electron column density within the eclipsing region. In both panels, there are observations at three frequencies: 0.732 GHz (triangle), 1.4 GHz (dots), and 3.1 GHz (circles).

the profile at 3.1 GHz is similar although the leading component appears to be weaker. At 0.732 GHz (observed away from superior conjunction), the trailing component has become the larger of the two. Strong pulse profile evolution has also been measured in other eclipsing systems, such as PSR J2215+5135 (Hessels et al. 2011). Further observations of PSR J1431−4715 at a range of frequencies will prove useful in both further study of the pulse profile evolution and measuring the spectral index.

This pulsar also exhibits significant orbital-phase-dependent delays in the pulse TOAs near superior conjunction (Fig. 4). The delays can be explained by an excess dispersion measure (DM), attributed to the passage of the radio pulses through ionized material surrounding the companion. The timing model described in Table 2 was generated by excluding TOAs which are obviously associated with the eclipse region, $0.1 < \Phi < 0.4$.

Multifrequency observations indicate that the magnitude of the eclipse delays depends upon observing frequency, with the 3.1 GHz observations showing somewhat shorter delays than at 1.4 GHz. Since this difference is removed when we convert from time delays to additional electrons along the line of sight, we can conclude that these delays are purely due to additional DM introduced by the material between the pulsar and Earth. The lower frequency observations (centred on 0.732 GHz) have not resulted in a positive detection to date across the eclipse region (see Fig. 4). Treating the delay as purely dispersive, we can relate the delay time, t, to the DM as

$$t = \frac{e^2}{2\pi m_e c} \frac{\mathrm{DM}}{f^2} \tag{5}$$

for observations at a frequency f. In Fig. 4, this DM has then been converted to the free-electron column density by approximating the depth of the eclipsing region as being equal to the radius of the eclipse region; the computed electron column density is similar to other eclipsing systems; for example PSRs J2051−0827 (Stappers et al. 1996) and J1731−1847 (Bates et al. 2011).

Using multiple observations during different eclipses, we find that there appear to be significantly different delays at the same orbital phase within the eclipse region. The TOAs were measured during observations which were separated by several months, that is $\sim 10^2$ orbital periods. As such, the amount, or density, of dispersive material must be variable on this time-scale. The width of the eclipsing region appears to be constant, suggesting that it is the free-electron density which is variable as opposed to depth of the eclipsing region.

From the orbital separation and the mass ratio, we determine the approximate distance of the Roche lobe from the companion, $R_{\rm L}$, using

$$R_{\rm L} = \frac{0.49Aq^{2/3}}{0.6q^{2/3} + \ln\left(1 + q^{1/3}\right)} \quad (6)$$

from Eggleton (1983), where A is the separation of the pulsar and its companion, and $q = m_{\rm c}/m_{\rm p}$ is the mass ratio of the system. In this case, $R_{\rm L} = 0.6\,{\rm R}_\odot$, about half the size of the eclipse radius.

A significant amount of the material in the eclipsing region is therefore outside the companion's Roche lobe. Material which is close to the Roche lobe can easily be removed by a relativistic pulsar wind (Breton et al. 2013). This would mean some eclipsing material was not gravitationally bound to the companion and must therefore be continually replenished (Stappers et al. 1996).

The spin-down dipole radiation $\dot{E}$ of the pulsar at the distance of the companion is $\dot{E}/A^2 \sim 1.5 \times 10^{33}{\rm erg\,s^{-1}\,ls^{-2}}$. This is typical of other eclipsing systems in general and in the HTRU sample (Roberts 2011; Breton et al. 2013). Incident spin-down energy at the companion is significantly larger for eclipsing systems than non-eclipsing binaries, an indication that the pulsar's energy output is at least partly responsible for the dispersive material surrounding the companion.

3.4 PSR J1653−2054

PSR J1653−2054 is a fully recycled MSP with $P = 4.129$ ms and $\dot{P} = 1.14 \times 10^{-20}$. The pulse profile at 1.4 GHz is shown in Fig. 2. The minimum mass of the companion to PSR J1653−2054 is just $0.08\,{\rm M}_\odot$, placing it between typical black widow and redback systems. The measurement of $\dot{E}/A^2 \sim 3.7 \times 10^{31}{\rm erg\,s^{-1}\,ls^{-2}}$ is however somewhat lower than for the redback and black widow systems (and PSR J1431−4715). It is, therefore, possible that the incident pulsar spin-down energy at the surface of the companion is too low to bloat the companion, which would explain why no eclipses have been observed. The orbital period is at least a factor of 2 longer than known Galactic redback and black widow systems (Roberts 2011). The wide orbit means that any ionized region would subtend a smaller angle, making eclipses less likely. If, however, the orbit is not being viewed edge-on then the companion mass would be higher, for instance, if $i < 25^\circ$, then $M_{\rm c} > 0.2\,{\rm M}_\odot$, indicative of a typical HeWD. A detection or constraint on the magnitude of the optical companion to this system may help us resolve the nature of the companion and whether this is an example of a wide orbit black widow or redback.

3.5 PSR J1729−2117

This system, with period $P = 66.29$ ms and period derivative $\dot{P} = 1.6 \times 10^{-19}$, has very similar spin parameters to PSR J0609+2130 (Lorimer et al. 2004) and PSR J2235+1506 (Camilo, Nice & Taylor 1993). Camilo et al. suggested that PSR J2235+1506 was spun-up in an HMXB system in which the second ccSN resulted in the disruption of the binary. It may be that similar arguments can be applied to PSR J1729−2117. As discussed by Burgay et al. (2013), this pulsar was only detected owing to an enhanced flux density due to scintillation during the discovery observation. Subsequent observations have revealed it to have a low luminosity (Table 2).

If this pulsar really was spun up in a binary, then PSR J1729−2117 might be expected to have a high velocity (Bailes 1989), and as the system is relatively close (the distance from NE2001 is $d = 1.09$ kpc), the proper motion should be measurable with further timing. Pulse profiles at 0.7, 1.4, and 3.1 GHz are shown in Fig. 2.

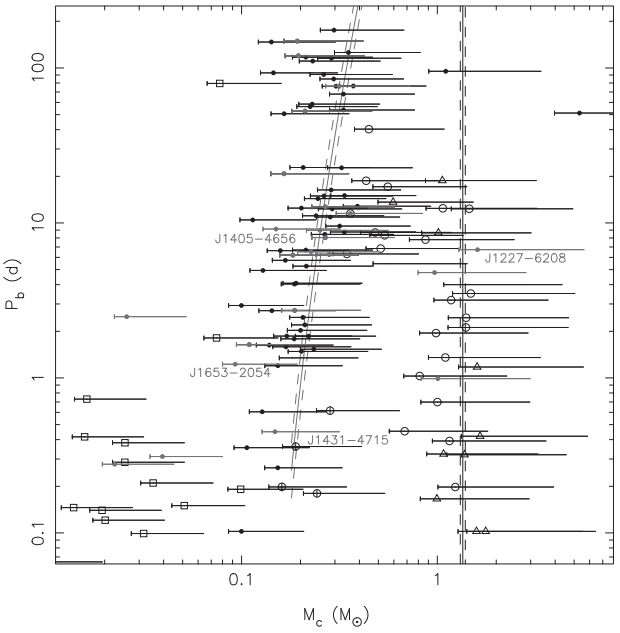

Figure 5. A plot of orbital period against companion mass for non-globular cluster pulsars. Data points correspond to the median mass value, while lower and upper limits correspond to the minimum companion mass and the 90 per cent confidence upper limit. The four binary systems presented in this paper are marked with text, and the other symbols correspond to the systems presented in Table 4. The curves indicate the relationship for HeWDs derived by Tauris & Savonije (1999) for three different companion progenitors, and the vertical lines denote a companion mass of 1.4 $M_\odot$, indicative of a DNS system.

3.6 Orbital periods and companion masses

The five MSPs presented here show quite diverse orbital properties. One, PSR 1729−2117, appears to be isolated and has presumably lost its companion at some point since it was recycled. Three pulsars, PSRs J1405−4656, J1431−4715, and J1653−2054, all have low- to intermediate-mass companions of $\sim$0.1–0.2 $M_\odot$, and finally PSR J1227−6208 has a high-mass companion of $\gtrsim 1.3\,{\rm M}_\odot$.

Tauris & Savonije (1999) derived a relationship between orbital period and companion mass for binary MSPs with WD companions which have formed via an LMXB phase (see Fig. 5). This relationship is based on a predictable core mass for a main-sequence star as a function of stellar radius. During spin-up in an LMXB, the edge of the star is at the position of the Roche lobe, which is a function of only the two masses and the orbital separation (see equation 6). After the companion star exhausts its fuel and the outer layers are blown off, the stellar core becomes a WD. The WD mass is therefore linked to the orbital period at cessation of mass transfer/spin-up.

Of the binary systems described here, PSR J1653−2054 has a shorter orbital period than those described by Tauris & Savonije (1999), who only considered $P_{\rm orb} \gtrsim 2$d. PSRs J1405−4656 and J1431−4715 are in agreement with this relationship, and since PSR J1227−6208 did not form via an LMXB phase, on which this relationship is based, it does not lie on the predicted curve. Indeed, its minimum companion mass is considerably higher than a low-mass WD.

3.7 Non-detection with the *Fermi* telescope

A large number of MSPs have been discovered by radio observations of point sources first identified by the Large Area Telescope (LAT) on board the *Fermi* Gamma-Ray Space Telescope (e.g. Cognard et al. 2011; Keith et al. 2011; Ransom et al. 2011). We searched the *Fermi* LAT second source catalogue (Nolan et al. 2012) for point sources which could be associated with the five newly-discovered pulsars presented here, but found no matches. Pulsar detections with *Fermi* are usually parametrized in terms of $\log(\sqrt{\dot{E}}/d^2)$ (for a spin-down energy loss, $\dot{E}$, measured in erg s^{-1} and distance, d, in kpc; see Abdo et al. 2010), which is usually $\gtrsim$17 for pulsars that are detected. For PSR J1431−4715, $\log(\sqrt{\dot{E}}/d^2) = 17$, so this pulsar might be considered to be right on the margins of detection by *Fermi*, if indeed the DM distance is correct. The other MSPs presented here all have values of $\log(\sqrt{\dot{E}}/d^2) \lesssim 16.5$.

4 POSSIBILITY OF OPTICAL DETECTION FOR HTRU MSP COMPANIONS

Observations of companions of binary pulsars can allow the determination of parameters which may not be measurable through pulsar timing alone. Of particular interest here are MSPs with low-mass helium-core WD companions, where a dichotomy in the thickness of the hydrogen envelope surrounding the helium-core of the WD leads to residual hydrogen burning, significantly slowing down the cooling (Alberts et al. 1996; Driebe et al. 1998; Althaus, Serenelli & Benvenuto 2001). As a result, helium-core WDs with masses below approximately 0.2 M$_\odot$ are typically intrinsically brighter than higher mass WDs. For those systems where the WD is bright enough for optical photometry, it is possible to measure its temperature and cooling age, providing independent constraints on the pulsar age (e.g. van Kerkwijk et al. 2000; Bassa, van Kerkwijk & Kulkarni 2003). Furthermore, if the WD has suitable absorption lines, phase-resolved optical spectroscopy of the WD can be used to determine the mass ratio and model the WD atmosphere to constrain both the WD and pulsar mass (e.g. van Kerkwijk, Bergeron & Kulkarni 1996; Callanan, Garnavich & Koester 1998; Bassa et al. 2006; Antoniadis et al. 2013 and see van Kerkwijk et al. 2005, for a review).

In Table 4, we present predictions for the apparent brightness of helium-core WD companions to MSPs discovered in the HTRU survey. The binary systems and their properties are listed in Table 4. We use predictions from WD cooling models from Bergeron, Wesemael & Beauchamp (1995) and Serenelli et al. (2001) to estimate the absolute magnitude by comparing the predicted WD cooling age with the characteristic spin-down age of the pulsar. The masses of the WDs are constrained through the timing measurements of the orbital period and projected semimajor axis. Assuming a pulsar mass of 1.4 M$_\odot$ and a range of probable orbital inclinations, we obtain the masses listed in Table 4.

Combining the observed pulsar dispersion measures with the NE2001 model of the Galactic electron distribution (Cordes & Lazio 2002) yields the distance estimates listed in Table 4. Since some of the HTRU MSPs are at low Galactic latitude, absorption can be significant. The Galactic extinction model of Amôres & Lépine (2005) was used to obtain estimates of the V-band absorption A_V for the distance to and line of sight of each MSP. Together, these provide the V-band distance modulus with which the apparent magnitude can be estimated.

Fig. 6 combines all these estimates; the characteristic spin-down age $\tau_{\rm c}$ of the pulsar with the predicted cooling age of the WD. As pulsar spin-down ages may not be a reliable age estimator for the pulsar (Tauris 2012), we conservatively compare a pulsar spin-down ages from $0.1\tau_{\rm c}$ to $\tau_{\rm c}$. The WD cooling models then predict the absolute V-band magnitude M_V. Combining these with the V-band distance modulus $(m - M)_V$ gives the predicted apparent V-band magnitude m_V. These estimates are also listed in Table 4.

Optical detection in imaging observations with an 8 m class telescope typically requires an apparent magnitude less than 24.

Table 4. Predicted optical magnitudes for the HTRU MSPs with helium-core WD companions. Limits are calculated using a lower limit on the pulsar spin-down age of $0.1\tau_{\rm c}$.

Name	d (kpc)	$\tau_{\rm c}$ (Gyr)	$M_{\rm c,\,med}$	A_V	$(m-M)_V$	M_V	m_V	Reference
J1017–7156	2.87	16.69	0.226	0.263	12.55	>13	>25.5	Keith et al. (2010)
J1056–7117	2.60	6.60	0.150	0.388	12.46	<10	<22.5	Ng et al. (2014)
J1125–5825	2.58	0.81	0.317	1.765	13.83	<13	<26.8	Bates et al. (2011)
J1405–4656	0.58	37.64	0.252	0.885	9.70	>16	>25.7	This paper
J1431–4715	1.53	2.26	0.148	2.290	13.21	>10	>23.2	This paper
J1431–5740	2.52	10.14	0.187	2.821	14.83	12–16	>26.8	Burgay et al. (2013)
J1528–3828	2.20	5.00	0.195	1.447	13.16	11–16	>24.2	Ng et al. (2014)
J1543–5149	2.43	2.02	0.268	4.413	16.34	10–14	>26.3	Keith et al. (2010)
J1545–4550	2.10	1.08	0.183	2.580	14.19	10–12	>24.2	Burgay et al. (2013)
J1708–3506	2.77	6.25	0.193	2.534	14.75	11–16	>25.8	Bates et al. (2011)
J1755–3716	3.90	6.40	0.360	0.400	13.36	11–16	>24.4	Ng et al. (2014)
J1801–3210	3.95	44.60	0.165	0.687	13.67	>10	>23.7	Bates et al. (2011)
J1811–2405	1.77	3.15	0.280	11.360	22.60	11–15	>33.6	Bates et al. (2011)
J1825–0319	3.03	10.61	0.211	9.210	21.62	>12	>33.8	Burgay et al. (2013)
J2236–5527	0.83	11.40	0.268	0.063	9.66	12–16	>21.7	Burgay et al. (2013)

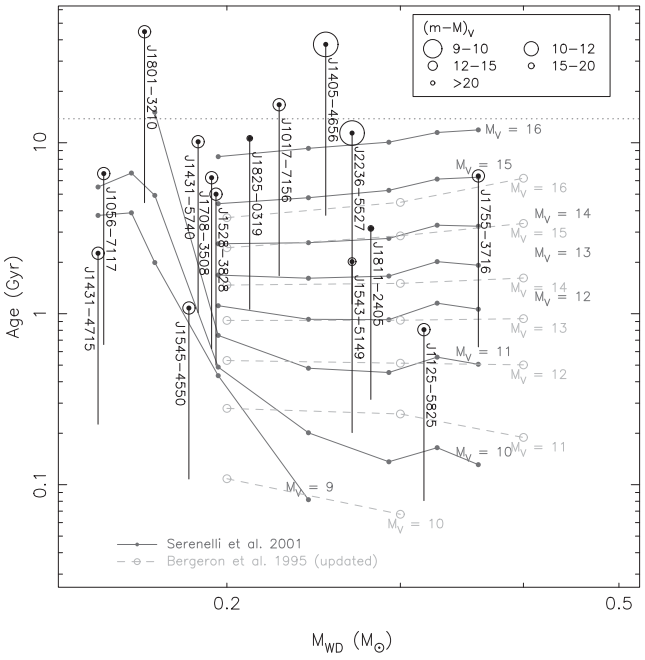

Figure 6. Comparing characteristic pulsar spin-down ages with WD cooling ages. Predictions of WD cooling age as a function of WD mass following the models by Bergeron et al. (1995, dashed lines/open circles) and Serenelli et al. (2001, solid lines/filled circles) are shown for a set of absolute *V*-band magnitudes M_V. Plotted with the filled circles are the estimated companion masses $M_{\rm c,\,med}$ (assuming a 1.4 $M_\odot$ pulsar and an $i = 60^\circ$ inclination) against the characteristic spin-down age $\tau_{\rm c}$ of the pulsar. The vertical line extends from the circles down to $0.1\tau_{\rm c}$ to denote a conservative range of pulsar ages. Finally, the size of the circles concentric with the dots denoting the characteristic pulsar age and companion mass, scales with the *V*-band distance modulus $(m - M)_V$, where larger circles indicate lower distance moduli. From the distance modulus and the absolute *V*-band magnitude, the apparent *V*-band magnitude for each companion for a given characteristic age can be calculated as $m_v = M_V + (m - M)_V$. The Hubble time is indicated by the dotted horizontal line at ∼14 Gyr.

For WDs brighter than 23rd magnitude, optical spectroscopy may be feasible provided suitable absorption lines are present in the spectrum. Based on the estimates from Table 4 and Fig. 5, the HTRU MSPs expected to have the WD companions that can be detected with 8 m class telescopes are PSRs J1056−7117, J1431−4715, and J2236−5527, especially if the characteristic pulsar age is an overestimate of the real age of the system. In the case of PSR J1125−5825, a detection may be possible if the characteristic age vastly overestimates the system's age.

5 SUMMARY

The discovery of five new MSPs from the HTRU survey has been presented. These pulsars represent members of a wide range of known recycled pulsar types, including possibly the heaviest WD known in orbit around an NS, an eclipsing redback system, and an isolated, mildly recycled pulsar, indicating that it probably came from a HMXB which was disrupted during the second ccSN.

Only one of these MSPs, PSR J1227−6208, is within the PMPS region. This pulsar was in fact co-discovered in recent re-analyses of the PMPS data (Mickaliger et al. 2012; Knispel et al. 2013). The superior temporal and spectral resolution of HTRU data means that even with shorter pointings (in the mid-latitude region) than PMPS, HTRU is able to discover MSPs initially missed by previous surveys which used similar instrumentation to PMPS (Edwards et al. 2001; Burgay et al. 2006; Jacoby 2009).

It would be interesting to attempt detections of some WDs in the HTRU sample in order to test the reliability of MSP spin-down ages. PSRs J1056−7117, J1125−5825, J1431−4715, and J2236−5527 are the most likely to result in positive detections. An optical observation of PSR J1431−4715 would also be informative for other reasons; if it is a redback system then its companion may be non-degenerate and it instead could be at the end of the spin-up phase (Roberts 2011). The companion may also be distinctly non-spheroidal, and measurements of an orbitally modulated light curve can constrain the inclination (Stappers et al. 2001; Reynolds et al. 2007). If spectroscopy as a function of orbital phase is possible for the companion then component masses can be constrained (van Kerkwijk, Breton & Kulkarni 2011; Romani et al. 2012).

ACKNOWLEDGEMENTS

The Parkes Observatory is part of the Australia Telescope which is funded by the Commonwealth of Australia for operation as a National Facility managed by CSIRO. We thank the reviewer, Dipankar Bhattacharya, for suggestions which helped improve the manuscript.

REFERENCES

Abdo A. A. et al., 2010, ApJS, 187, 460
Alberts F., Savonije G. J., van den Heuvel E. P. J., Pols O. R., 1996, Nature, 380, 676
Alpar M. A., Cheng A. F., Ruderman M. A., Shaham J., 1982, Nature, 300, 728
Althaus L. G., Serenelli A. M., Benvenuto O. G., 2001, MNRAS, 324, 617
Amôres E. B., Lépine J. R. D., 2005, AJ, 130, 659
Antoniadis J. et al., 2013, Science, 340, 448
Archibald A. M. et al., 2009, Science, 324, 1411
Bailes M., 1989, ApJ, 342, 917
Bassa C. G., van Kerkwijk M. H., Kulkarni S. R., A&A, 403, 1067
Bassa C. G., van Kerkwijk M. H., Koester D., Verbunt F., 2006, A&A, 456, 295
Bates S. D. et al., 2011, MNRAS, 416, 2455
Bates S. D. et al., 2012, MNRAS, 427, 1052
Bergeron P., Wesemael F., Beauchamp A., 1995, PASP, 107, 1047
Bhattacharya D., van den Heuvel E. P. J., 1991, Phys. Rep., 203, 1
Boyles J. et al., 2013, ApJ, 763, 80
Breton R. P. et al., 2013, ApJ, 769, 108
Burgay M. et al., 2003, Nature, 426, 531
Burgay M. et al., 2006, MNRAS, 368, 283
Burgay M. et al., 2013, MNRAS, 433, 259
Callanan P. J., Garnavich P. M., Koester D., 1998, MNRAS, 298, 207
Camilo F., Nice D. J., Taylor J. H., 1993, ApJ, 412, L37
Camilo F. et al., 2001, ApJ, 548, L187
Chaurasia H. K., Bailes M., 2005, ApJ, 632, 1054
Cognard I. et al., 2011, ApJ, 732, 47
Cordes J. M., Lazio T. J. W., 2002, preprint (astro-ph/0207156)
D'Amico N., Lyne A. G., Manchester R. N., Possenti A., Camilo F., 2001, ApJ, 548, L171
Dewi J. D. M., Podsiadlowski P., Pols O. R., 2005, MNRAS, 363, L71
Driebe T., Schoenberner D., Bloecker T., Herwig F., 1998, A&A, 339, 123
Eatough R. P., Molkenthin N., Kramer M., Noutsos A., Keith M. J., Stappers B. W., Lyne A. G., 2010, MNRAS, 407, 2443
Edwards R. T., Bailes M., van Straten W., Britton M. C., 2001, MNRAS, 326, 358
Eggleton P. P., 1983, ApJ, 268, 368
Eichler D., Levinson A., 1988, ApJ, 335, L67
Freire P. C. C., Wex N., 2010, MNRAS, 409, 199

Fruchter A. S., Stinebring D. R., Taylor J. H., 1988, Nature, 333, 237
Hessels J. W. T. et al., 2011, in Burgay M., D'Amico N., Esposito P., Pellizzoni A., Possenti A., eds, AIP Conf. Proc. Vol. 1357, Radio Pulsars: An Astrophysical Key to Unlock the Secrets of the Universe. Am. Inst. Phys., New York, p. 40
Hobbs G. B., Edwards R. T., Manchester R. N., 2006, MNRAS, 369, 655
Hulse R. A., Taylor J. H., 1975, ApJ, 195, L51
Jacoby B. A., Bailes M., Ord S. M., Edwards R. T., Kulkarni S. R., 2009, ApJ, 699, 2009
Keith M. J. et al., 2010, MNRAS, 409, 619
Keith M. J. et al., 2011, MNRAS, 414, 1292
Knispel B. et al., 2013, ApJ, 774, 93
Lange C., Camilo F., Wex N., Kramer M., Backer D. C., Lyne A. G., Doroshenko O., 2001, MNRAS, 326, 274
Lorimer D. R. et al., 2004, MNRAS, 347, L21
Lyne A. G. et al., 2004, Science, 303, 1153
Manchester R. N. et al., 2001, MNRAS, 328, 17
Manchester R. N., Hobbs G. B., Teoh A., Hobbs M., 2005, AJ, 129, 1993
Mickaliger M. B. et al., 2012, ApJ, 759, 127
Migliazzo J. M., Gaensler B. M., Backer D. C., Stappers B. W., van der Swaluw E., Strom R. G., 2002, ApJ, 567, L141
Ng C. et al., 2014, MNRAS, 439, 1865
Nolan P. L. et al., 2012, ApJS, 199, 31
Papitto A. et al., 2013, Nature, 501, 517
Phinney E. S., 1992, Phil. Trans. R. Soc. A, 341, 39
Ransom S. M. et al., 2011, ApJ, 727, L16
Reynolds M. T., Callanan P. J., Fruchter A. S., Torres M. A. P., Beer M. E., Gibbons R. A., 2007, MNRAS, 379, 1117
Roberts M. S. E., 2011, in Burgay M., D'Amico N., Esposito P., Pellizzoni A., Possenti A., eds, AIP Conf. Proc. Vol. 1357, Radio Pulsars: An Astrophysical Key to Unlock the Secrets of the Universe. Am. Inst. Phys., New York, p. 127
Romani R. W., Filippenko A. V., Silverman J. M., Cenko S. B., Greiner J., Rau A., Elliott J., Pletsch H. J., 2012, ApJ, 760, L36
Ruderman M., Shaham J., Tavani M., 1989, ApJ, 336, 507
Serenelli A. M., Althaus L. G., Rohrmann R. D., Benvenuto O. G., 2001, MNRAS, 325, 607
Shapiro I. I., 1964, Phys. Rev. Lett., 13, 789
Shklovskii I. S., 1970, SvA, 13, 562
Stappers B. W. et al., 1996, ApJ, 465, L119
Stappers B. W., van Kerkwijk M. H., Bell J. F., Kulkarni S. R., 2001, ApJ, 548, L183
Stappers B. W. et al., 2014, ApJ, 790, 39
Tauris T., 2012, Science, 335, 561
Tauris T. M., Savonije G. J., 1999, A&A, 350, 928
Tauris T. M., van den Heuvel E. P. J., in Lewin W. H. G., van der Klis M., eds, Formation and Evolution of Compact Stellar X-ray Sources. p. 623
Tauris T. M., Langer N., Kramer M., 2012, MNRAS, 425, 1601
Toscano M., Sandhu J. S., Bailes M., Manchester R. N., Britton M. C., Kulkarni S. R., Anderson S. B., Stappers B. W., 1999, MNRAS, 307, 925
van Kerkwijk M. H., Bergeron P., Kulkarni S. R., 1996, ApJ, 467, L89
van Kerkwijk M. H., Bell J. F., Kaspi V. M., Kulkarni S. R., 2000, ApJ, 530, L37
van Kerkwijk M. H., Bassa C. G., Jacoby B. A., Jonker P. G., 2005, in Rasio F. A., Stairs I. H., eds, ASP Conf. Ser. Vol. 328, Binary Radio Pulsars. Astron. Soc. Pac., San Francisco, p. 357
van Kerkwijk M. H., Breton R. P., Kulkarni S. R., 2011, ApJ, 728, 95
Wijnands R., van der Klis M., 1998, Nature, 394, 344

This paper has been typeset from a TEX/LATEX file prepared by the author.